The International Journal of Advanced Manufacturing Technology (2019) 101:3183–3197
https://doi.org/10.1007/s00170-018-3162-8

ORIGINAL ARTICLE

Investigation on the effect of heat treatment and process parameters on the tensile behaviour of SLM Ti-6Al-4V parts

Amir Mahyar Khorasani [1,2] · Ian Gibson [1,3] · Alireza Ghaderi [4] · Mazher Iqbal Mohammed [1]

Received: 29 May 2018 / Accepted: 6 December 2018 / Published online: 18 December 2018

Abstract

Additive manufacturing (AM) has various independent parameters that affect the mechanical properties and quality of the produced parts that are not linearly the function of each other. Process parameters in metal AM are very hard to control, analyse and optimise because they affect each other even though they can be independently changed. Changing process parameters in a wide range is not possible due to the formation of problems such as cracks, balling, unmelted powders, porosity and distortion. In this paper, a numerical model to predict the value of tensile strength of selective laser melting (SLM) Ti-6Al-4V parts and analyse the effect of process parameters on the results has been proposed. Taguchi L25 Design of Experiment (DOE) across 125 samples to create a comprehensive and general overview of influential parameters on the build process was investigated. Specifically, parameters included laser power, scan speed, hatch spacing, laser pattern angle and heat treatment (HT). To evaluate and analyse the build process according to established statistical variances, a minimum of five samples based on ASTM standard (for tensile test) were prepared. Heat treatment was added to the DOE to analyse the combined process and post-process effects. Results were compared (cross-validated) against existing values found in the literature and were found to effectively predict and explain the behaviour of tensile strength when changing process parameters.

Keywords Selective laser melting · Mechanical properties · Additive manufacturing · Tensile properties · Heat treatment

1 Introduction

Additive manufacturing (AM) has seen extensive use in both academia and industry due to the ability to produce complex geometries unattainable by the majority of traditional manufacturing methods and to do so in a single production phase. In particular, metal-based printing techniques such as selective laser melting (SLM) [1] and electron beam melting (EBM) [2] are growing in popularity due to the promise of constructing functional parts for applications in aerospace [3, 4], automotive [5] and medical [6] industries. Despite this promise, application of metal AM parts is hindered by poor surface finish [1], dimensional deviation from the original computer model and differing mechanical properties compared to conventional manufacturing processes.

With respect to SLM, such issues can be traced back to suboptimised build processes, leading to the unstable melt-pool formation, unmelted particles, poor particle fusion and 'volcano' effects. These can lead to microporosity, cracks, key-holes, residual particles, delamination, distortion and staircase effect, thus negatively impacting a part's mechanical properties [7]. Teng et al. [8] provided a review of defect modelling in laser AM build processes, categorising defects into two primary

✉ Amir Mahyar Khorasani
a.khorasani@deakin.edu.au

Ian Gibson
i.gibson@utwente.nl

Alireza Ghaderi
a.ghaderi@deakin.edu.au

Mazher Iqbal Mohammed
mazher.mohammed@deakin.edu.au

[1] School of Engineering, Deakin University, Waurn Ponds, Victoria, Australia

[2] Department of Mechanics of Solids, Surfaces & Systems, Faculty of Engineering Technology, University of Twente, Enschede, The Netherlands

[3] Fraunhofer Centre for Complex System Engineering, Department of Design, Production and Management, University of Twente, Enschede, The Netherlands

[4] Institute for Frontier Materials, Deakin University, Waurn Ponds, Victoria, Australia

subgroups of porosity (balling and keyholes)- or crack (residual stress and lack of fusion)-related origins. Gong et al. [9, 10] provided a more fundamental understanding of defect formation during the build process and the influence on mechanical properties. They characterised these as mass transfer, vaporisation, melt pool discontinuity and process instability phenomena. More specifically, mass transfer can result from excess in imparted thermal energy from the laser, resulting in a recoil pressure in the melt pool. This in turn leads to uncontrolled ejection of molten material. This material subsequently undergoes rapid solidification leading to the welding of small spherical particles on the upper build surface. If the welded material is larger than the designated build layer thickness, they can be dislodged by the powder recoating blade, leaving behind a small pit in the build layer resulting in a porous region within the bulk of a part. Process instability relates to the inherent system performance and builds precision. For instance, fluctuations in laser power can result in variations in thermal energy impartation beyond predicted expectations. Equally, issues relating to low energy density (low beam power, high scan speed) or unoptimised hatch spacing (beam overlap), can result in a lack of melt pool wetting or unmelted powder, resulting in voids and porous regions. Finally, vaporisation effects result in the creation of gas bubbles which are the precursor mechanism for microvoids and keyhole formations. These issues can be largely attributed to a lack of parameter optimisation and ultimately result in parts with compromised mechanical properties.

To manipulate the mechanical properties of as-built samples, several methodologies [11] have been used. In the SLM build process of Al12Si, changes in hatch strategy and preheating have resulted in variations of part surface morphology and tensile properties. This was attributed to changes in the crack propagation path. Also, preheating of substrate showed improvement in ductility at the expense of strength. Using different hatch styles, preheating and contours allowed for the tailoring of tensile properties [11]. Build direction affects microstructure, mechanical properties and surface quality. The tensile properties in the Z direction (vertical building direction) were found to be lower for higher thermal gradients and cooling rates due to larger occurrences of pores and cracks [12, 13].

Heat treatment also changes the mechanical properties of metallic AM parts. For Ti-6Al-4V, thermally induced phase transformation provided the best combination of ductility, strength and hardness. Increasing the holding temperature results in α phase coarsening and decreasing strength. Increasing heat treatment temperature in the range of $\alpha + \beta$ leads to increasing the percentage of β and formation of equiaxed microstructure and a significant increase in elongation. In annealing, $\alpha + \beta$ precipitation of beta on α' leads to a decrease in tensile strength and improving ductility [14, 15]. A new investigation [16] of tensile properties of Ti-6Al-4V showed that annealing at 800 °C for 6 h results in removing twins and dislocations. Ultimately, it was found that the developed annealing protocol resulted in a fully decomposed lamellar microstructure, leading to a stronger and more ductile build structure with mechanical performance similar to wrought Ti-6Al-4V. Cai et al. [17] showed that SLM of Ti-6Al-4V coupled with hot isostatic pressure (HIP) showed improving breaking elongation from 5 to 15% while tensile strength decreased 20%. Increasing HIP temperature showed higher compatibility of the crystallographic features at the interfaces.

SLM of Mg showed both preheating, and layer thickness increased the value of hardness and elastic modulus so that they were similar to human bone [18]. In another study by Yadroitsev et al. 2012, [19] thermal transfer in the solid/liquid phase was found to be a key factor in solidification and the resulting part mechanical properties for 316 L stainless steel. Using lower scan speed and preheating results in the fabrication of coarser structures as these two factors influence the remelted depth. The scan speed controls the track width and height while the effect of preheating is more dominant at 0.5 T_{melt} and inappropriate selection of these parameters may result in Rayleigh instability, balling and track instability, thereby producing samples of lower quality.

When considering the build process, the scan parameters dominate several mechanisms affecting build optimisation. Analysing the process parameters on density and defect distribution of Cu-Al-Ni-Mn showed that scan strategy is the dominant factor in pore size and distribution, which relates to heat flow during solidification. Additionally, remelting of the previous solidified layer can be used to eliminate pores and generate more equiaxed grains, which combined improves the relative density [20]. Crack initiation is also related to scanning, where a lack of optimisation of the laser overlap area leads to the formation of cleavage steps along points of tensile loading. The scanning strategy affects the sliding surface from track to track and layer to layer, resulting in changes in tensile properties. Combined optimisation of track to track and layer to layer sliding surfaces result in the generation of excellent tensile strength [21].

Powder morphology also has a profound impact on the SLM build process, where generally smaller powders have been found to yield improved mechanical properties. When using larger powders, micropores were more prevalent in build layers resulting in reductions in tensile strength. It should also be noted that this is interrelated with optimisation of laser power, where reduced thermal penetration within the resulting thicker layers leads to reduced remelting and consolidation, thereby exacerbating inhomogeneity in the build material and increasing the chance of cracks and pores. Cracks generated by this process are generally found to be orientated along the layer axis and so external loads perpendicular to these layers readily cause fracture [22]. Contrary to the goal of increased mechanical properties, Taguchi methods have

been applied to control the porosity in such a way as to reduce the elastic modulus from 248 to 120 and 110 to 40 GPa for Co-Cr and Ti respectively. Interesting in this instance is that the deliberate reduction in elastic modulus can be tailored to match that of human bone, simply by changing process parameters and using lattice structures, yielding many exciting possibilities for biomedical implants [23].

Ultimately, a thorough analysis of build process parameters is required to control physical phenomena such as melting, solidification, vaporisation, periodic heating and cooling dynamics, to increase the build efficiency in SLM. Examination of the current literature has revealed that efforts have been focused on single parameter analyses, while many of these deal with the prediction of mechanical properties. Results are therefore not directly expandable and transferable to other machines due to lack of test samples, repetition and real-time analysis [24].

In response to these challenges, this study will apply artificial neural networks (ANN) to model, predict and analyse the simultaneous influence of multiple build parameters on the SLM process. Taguchi L25 approach was utilised, where outcomes are determined using five repetitions of a printed sample variant. Build parameters of interest included laser power, scan speed, hatch space, scan pattern angle and heat treatment. The contribution of each factor as well as the interaction of factors on tensile strength were analysed and fully discussed.

2 Experimental set-up

2.1 Powder material and SLM operation

Samples were printed based on ASTM E8 and E8M (Sub-size Specimen) using an SLM 125HL (SLM Solutions GmbH, Lubeck, Germany) machine, equipped with YLR-Fibre-Laser with a minimum spot size of 5 μm [25]. Samples were printed horizontally. Table 1 shows the SLM build parameters and specifications which were constant during a test and these were selected based on manufacturer recommendations. Samples were fabricated using Ti-6Al-4V powder in the form of standard tensile tests coupons. Figure 1**a** illustrates a magnification of the Ti-6Al-4V powder used in this study, Fig. 1**b** illustrates data on the powder particle size distribution, while Fig. 1**c** shows examples of the tensile test coupons manufactured in this study.

Table 1 SLM constant process parameters

System parameters	Value
Min. scan line/wall thickness	120 μm
Operational beam focus variable	100 μm
Layer thickness	30 μm
Laser spot diameter	0.2 mm

2.2 Design of experiment

In this experiment, five influential build parameters simultaneously were examined. The number of tests that could be performed would be unrealistic both in terms of time and the cost for evaluating every permutation. In order to reduce the number and cost of the experiments while retaining experimental accuracy, a Taguchi Design of Experiment (DOE) was implemented [26]. More specifically, a Taguchi L25 was selected that relates to the existence of five factors across five levels, as outlined in Table 2. To address statistical variations, five repetitions for each sample were chosen. Therefore, 125 samples were printed and tested to generate a comprehensive set of results. Factors in each column have to be analysed independently and therefore the number of replications in each column is balanced. In this case, the design is stated as orthogonal. The process parameters and their values are presented in Table 2.

2.3 Post-processing (heat treatment)

The periodic cooling and heating during the build processes and the resulting large thermal gradients lead to parts with low ductility and high tensile strength. To enhance the ductility and machinability of the parts, different annealing processes followed by furnace cooling have been used [1, 27]. Table 3 shows the heat treatment conditions that were used in this experiment. Stress relieving leads to removal of the generated thermal stresses due to periodic cooling and heating. Mill annealing is the removal of α'-martensite to improve ductility. $\alpha + \beta$ annealing results in the formation of globular microstructures and therefore better ductility. To further increase the ductility, β annealing is carried out [14]. In all instances, the heating and resident time were fixed at 120 mins and so the heating gradient steadily increased from ambient to the different set temperatures at rates of 4.8–8.6 °C/min. The cooling rate was kept fixed at 5 °C/min across all samples to prevent a detrimental impact to the mechanical properties [28].

2.4 Tensile testing

Tests were carried out using an Instron 8801-100kN machine equipped with hydraulic jaws to determine ultimate tensile strength and percentage of elongation. Axial gauge length and test rate were selected as 31.05 mm and 2 mm/min respectively. The results are shown in the Appendix Table 5. Appendix Figure 10 shows the stress strain curve for five samples with all different heat treatment temperatures.

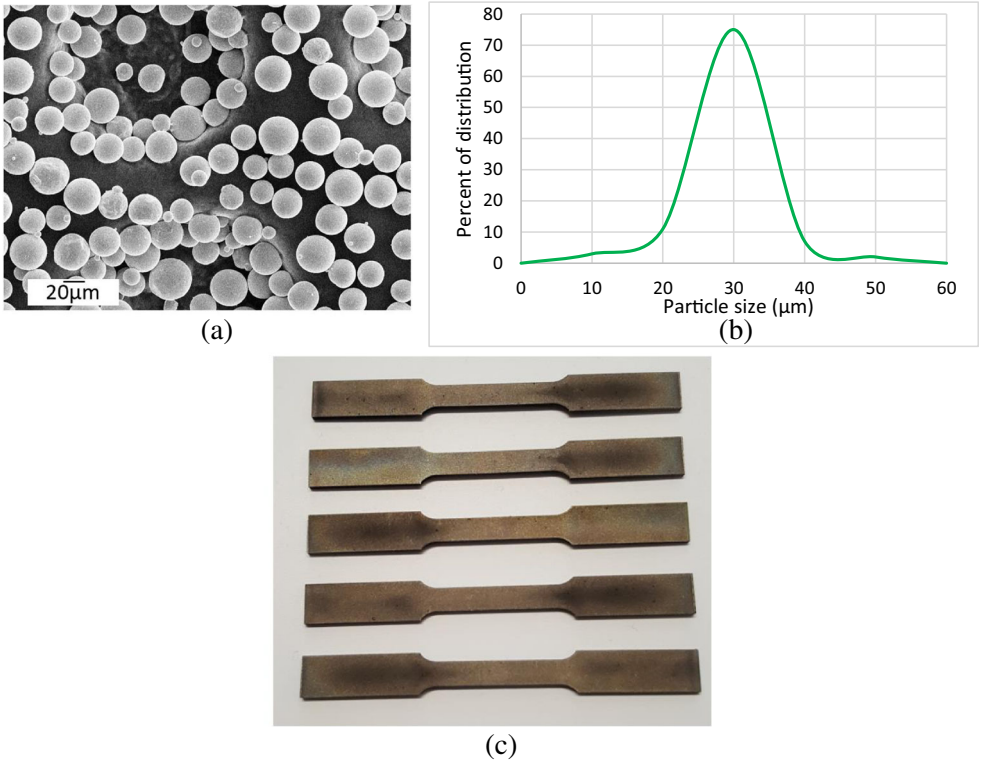

Fig. 1 **a** Powder; **b** particle size distribution; **c** printed samples

3 Modelling

3.1 Neural network model

ANNs have long seen a wide variety of applications in industrial, medical, marketing and banking systems to solve complex system behaviours [29]. With respect to numerical modelling and forecasting, ANNs are able to predict/estimate the outputs from complex multi-parameter-based problems, such as those seen in the SLM build process. ANN is a framework for many different machine learning algorithms to work together and process complex data inputs to solve problems in a similar way that a human brain would. When outputs are not a linearly separable combination of inputs, multi-layer perceptron (MLP) is a fast and accurate application for function approximation [30]. These networks use supervised learning methods called "backpropagation" for network training. The inputs of the ANN were laser power, scan speed, hatch space, laser pattern angle and heat treatment. Qnet 2000 software was used for this model which has the ability of modelling and analysing the effective process parameters on the results and is well-known to model industrial processes [31, 32]. Using an initial prediction, which is then validated using experimental test data, the network begins training in the first steps towards wider system predictive understanding. Following this initial round of prediction, the ANN uses a recall procedure incorporating the new experimental data to determine the validity and accuracy of the network, before commencing on subsequent rounds until predictions match those of experimental outcomes to a high degree of correlation.

In this research due to the non-linear relationship between build process parameters and outputs, multi-layer perceptron ANNs have been used to model the process. To increase the accuracy of the proposed ANN, cross-validation has been carried out using five prediction rounds across all 25 examined data points in the study.

Table 2 Process parameters and levels

Laser power (W)	Scan speed (mm/min)	Hatch spacing (μm)	Scanning pattern incrementing angle (^{0})	Heat treatment temperature C^0
90	600	65	36	20
95	650	70	40	600
100	700	75	45	750
105	750	80	60	925
110	800	85	75	1050

4 Results and discussion

4.1 Results of the cross-validation

The results of cross-validation can be seen in Table 4. It is shown that higher than 80% correlation was obtained for all five cross-validations for recall process that confirms the

Table 3 Heat treatment condition (20 means no heat treatment)

Commercial name	Temperature (C)	Heating time (min)	Resident time	Cooling time (min)
As-built	20	–	–	–
Stress relieving	600	120	120	120
Mill annealing	750	120	120	150
α + β annealing	925	120	120	185
β annealing	1050	120	120	210

designed network is working accurately and has acceptable generality. The average contribution of train, test and recall for all cross-validations also shows 100%, 82.01% and 88.21% correlation respectively that proves the reliability of the proposed ANN.

4.2 Statistical analysis for correlation of input on tensile values

The numerical results of the modelling are shown in Fig. 2**a**–**j**. Figure 2**a**, **c**, **e**, **g**, **i** show a very good correlation of experimental values and ANN predictions demonstrating the efficacy of the proposed ANN. In Fig. 2**b**, **d**, **f**, **h**, **j**, the recall procedure for all five cross-validations showed a general trend that predicted the tensile strength for a respective cross-validation stage, albeit with a minor discrepancy in between the predicted and measured absolute tensile strength by the proposed network. This figure proves that the designed network was trained in the right order and works properly.

Table 4 Results of the cross-validation

Cross-validation	Process	Std Dev	Max error	Correlation
First	Training	0.06338	0.1665	100
	Test	159.584	211.822	91.276
	Recall	126.3903	188.4406	91.306
Second	Training	0.15036	0.3291	100
	Test	212.6783	261.5244	83.829
	Recall	117.9162	156.9789	83.558
Third	Training	0.229	0.63629	100
	Test	158.4196	260.5638	74.281
	Recall	81.02818	127.4597	92.364
Fourth	Training	0.05851	0.15332	100
	Test	190.3347	310.4224	71.638
	Recall	142.7079	244.2268	88.738
Fifth	Training	2.95414	7.8775	99.986
	Test	146.0749	204.66	89.031
	Recall	158.7935	228.9528	85.062

4.3 Average contribution of input nodes on outputs using ANN

Modelling of the SLM build process of Ti-6Al-4V is dictated by a strong understanding of melt pool dynamics, which is largely related to thermal control mechanisms. The challenge when processing Ti-6Al-4V is its low intrinsic thermal conductivity, which results in complex melt pool behaviours when compared to materials such as stainless steel [33, 34]. To analyse the effective parameters, interrogator analysis using ANN has been carried out. The interrogator analysis has been done five times for all cross validations to show which parameter is more influential on the value of tensile properties. Figure 3 shows the interrogator analyses for all cross-validations. Of all the parameters interrogated, it was found that the laser power had the highest influence on the value of tensile strength. Depending on the selection of the other parameter values, any number of these could be seen to have secondary influence, thus highlighting the challenges of modelling.

4.4 Interaction of process parameters on tensile values

Ti-6Al-4V is quite sensitive to internal stresses within the process. However, Ti-6Al-4V has low thermal conductivity and this leads to accumulation of higher heat and lower "lack of melting" problems compared with stainless steel and also has a more complex behaviour regarding microstructure and mechanical properties [33].

Therefore, to derive trends of complex behaviour in AM, contour plots based on the result of the training process in ANN were drawn and analysed. Pre-process, process and post-process parameters affect the porosity, microstructure and subsequently the tensile properties of printed parts. In this section, the effect of process parameters such as laser power, scan speed, hatch space and pattern angle as well as post-process heat treatment temperature on tensile properties are discussed.

4.4.1 Interaction of laser power versus other parameters

Figure 4**a**–**d** show a contour plot for laser power against each of the other interrogated parameters. In this research, laser power was found to be the most influential factor on tensile strength and roughness measurements showed that this parameter is the most effective factor on the quality of the surface, confirming Pupo's investigations [35]. It was ultimately found that by decreasing laser power the tensile strength improved, where for powers lower than 100 W the tensile strength was found to be > 1GPa. There are several potential reasons for this. The surface condition can have a significant effect on mechanical properties such as fatigue and tensile behaviour. This is related to layer-layer effect and generation of pores including microcracks, keyholes, lack of fusion,

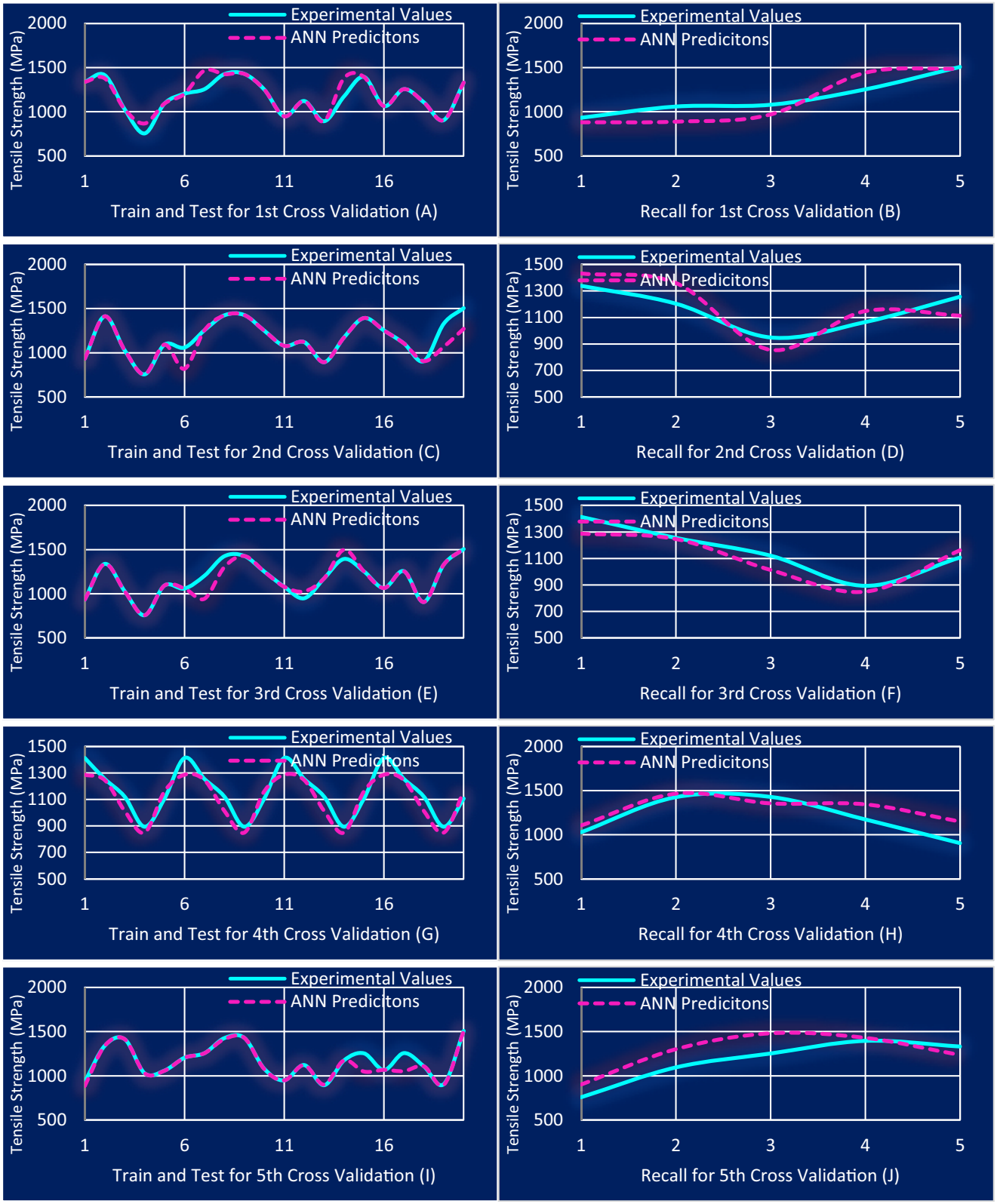

Fig. 2 Results of ANN modelling for each cross-validation

boiling and volcano effect [36]. Surface quality is ultimately related to melting pool size and energy density. Higher laser energy leads to partial melting over a wider area and overflows at the surface, resulting in increased porosity [37]. This behaviour can be explained by an energy density equation, where it is shown that temperature is a direct function of

laser power. Therefore, increases in laser power increase the melt pool recoil pressure, resulting in instabilities that lead to increased porosity. The width of the scanning track is related to laser power and scan speed as well as the interaction of these two parameters. When using higher laser power and lower scan speed (Fig. 4a), the melting pool becomes wider and temperature increases. Beyond a critical point, the centre of the melt pool can exhibit Marangoni's effects, transferring heat towards neighbouring build regions. Consequently, a melt pool region of partial solid and liquid material (mushy region) forms. Due to higher viscosity in mush area [27], the gradient for melting flow is zero; therefore, higher temperature stores in these regions, leading to increased thermal stress, and decreasing surface tension (Marangoni's effect)

If T_0 is initial temperature and T_c is critical temperature, then the ratio of κ in Eq. 1 shows that increasing temperature leads to an increase of κ [38, 39]:

$$\kappa = \frac{T - T_0}{T_c - T_0} \tag{1}$$

At the critical temperature, according to Eq. 2, the surface tension becomes zero. However, in SLM, the working temperature for Ti-6Al-4V reaches to maximum 2200 °C while surface tension decreases to zero at 3560 °C (which is Ti-6Al-4V boiling temperature). Therefore, in SLM, surface tension never reaches zero value (except for surface vaporisation).

$$\gamma = \sqrt[3]{\frac{1^2}{v_l}}\,(T - T_c) \tag{2}$$

where v_l is molar volume. Increasing κ in Eq. 1 leads to decreasing surface tension due to thermo-capillary effect and this phenomenon is called Marangoni's effect that is shown in Eq. 3 [38, 39].

$$\gamma = \gamma^* \left(\frac{T_c - T_0}{T_c}\right)[1 - \kappa] \tag{3}$$

where γ^* is constant for each liquid. Higher laser power leads to higher penetration of laser beam, so the interaction of (surface tension force + hydrostatic force) versus vapour pressure is not balanced and keyholes were appeared which affect the mechanical properties [40].

During manufacturing, irregularity of layer tracks was observed for samples fabricated at lower scan speeds, resulting in reduced tensile strength. When the scan speed increased, tensile strength also increased, as can be seen in areas 1 and 2, Fig. 4**a**, and which is in agreement with the literature [41]. It is worth noting that a small reduction on tensile value is observed in Fig. 4**a** (zone 4), which can be explained by the greater effect of laser power on tensile strength (Fig. 3). The largest tensile strength was obtained at laser powers ranging between 93 and 100 W. This however decreased rapidly towards the lowest laser power (90 W) and is believed to be due to a lack of powder fusion, which is exacerbated at higher scan speeds due to the lower energy density. Similarly, Qiu et al. [42] found that increasing scan speed results in the more stable melting pool and subsequent continuous and homogeneous material which improves the strength.

Ultimately, the SLM process is sensitive to energy input values. It was found that insufficient energy density is more influential in governing mechanical properties as compared to the samples with excessive energy input. The lack of energy input fundamentally results in unmelted regions, leading to the generation of pores and cracks and the subsequent reduction of tensile properties [2]. Figure 5 illustrates one such instance discovered in the test samples, where a clear lack of powder fusion has generated a large pore within the bulk of the samples. In addition, when increasing laser power

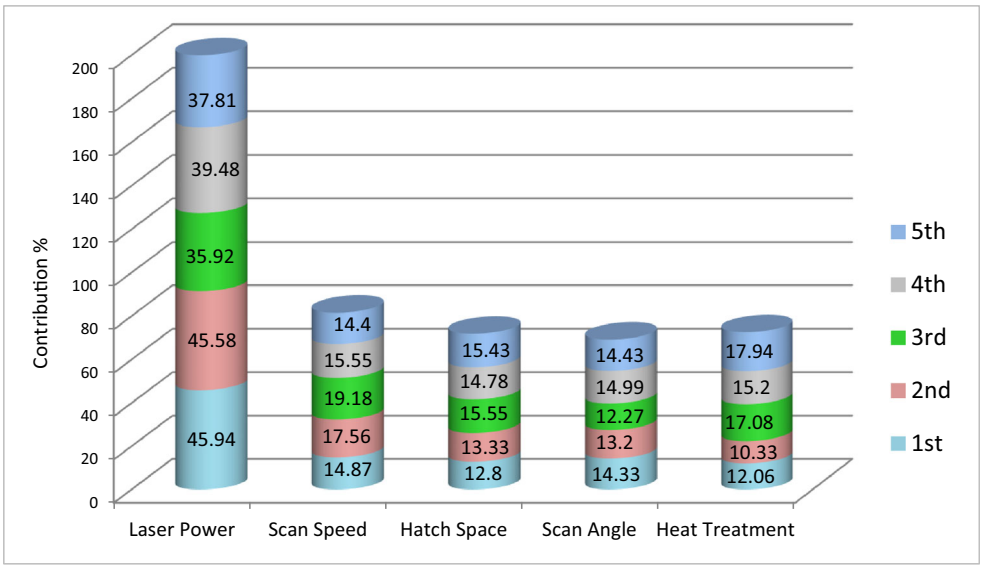

Fig. 3 Contribution of inputs on the results for all five cross-validations

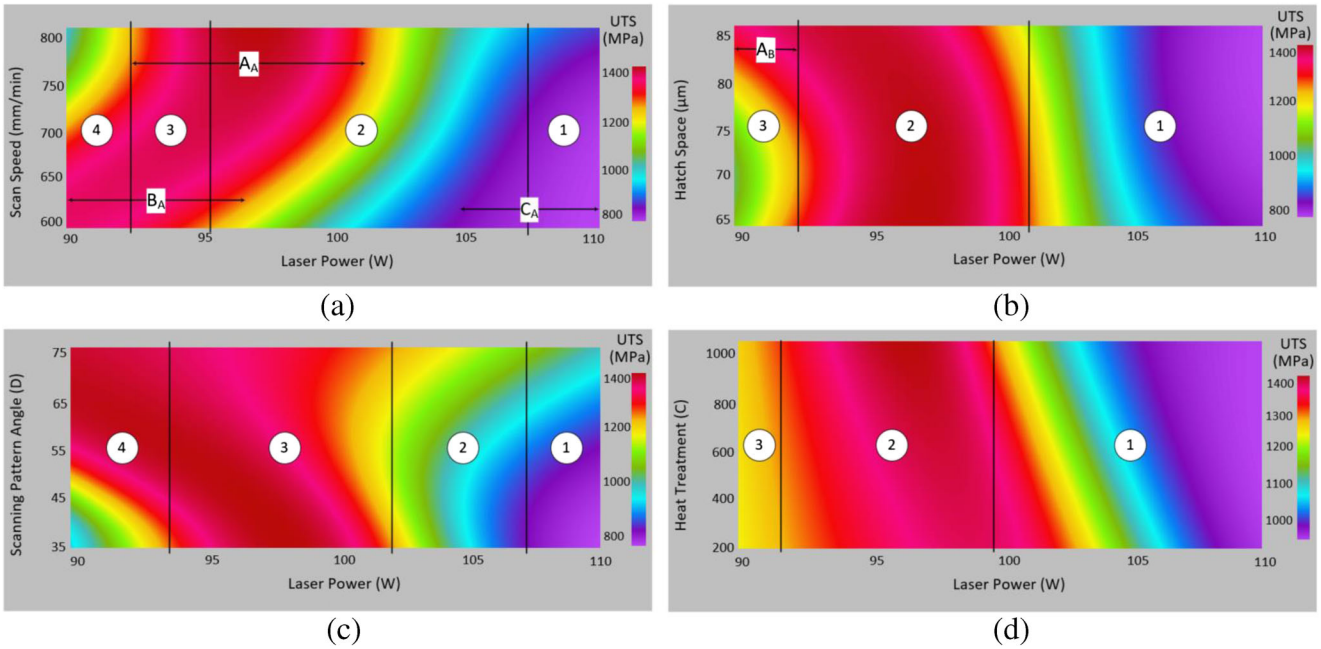

Fig. 4 Interaction of laser power on other parameters. **a** Scan speed; **b** hatch space; **c** scanning pattern angle; **d** heat treatment

and decreasing scan speed, the temperature of melt pool increases and higher Marangoni's effects and flow were observed. This causes instability in melting pool; therefore, unmelted powders move into the melt pool and more waves are generated and fast cooling rate in laser-based AM, ultimately leading to the formation of defective layer surfaces and decreased tensile strength (Fig. 4**a** region C_A). Increasing laser power tends to generate higher temperature on the melting pool. It was reported that in SLM of Ti-6Al-4V spherical porosity is related to trapped gas under melting pool during solidification [27]. Therefore, in higher laser power, higher porosity and less strength were observed. In addition, during high-speed scanning, balling is found due to low wettability, reduction in contact between substrate and melt and Rayleigh instability.

Figure 4**b** shows increased tensile strength was obtained for laser powers between 94 and 98 W across all examined hatch spacing's (region 2). This can be explained again due to the decreased temperature resulting in a subsequently smaller mushy area and the keyhole effect. The insignificant effect of hatch spacing on tensile properties once again confirms the validity of the ANN prediction according to Fig. 3. Examining region 3 of Fig. 4**b** shows that by increasing hatch space from 65 to 85 μm the value of tensile strength increased by 40%. As the overlapping area is a direct function of hatch spacing, higher hatch spacing generates lower overlap, and results in

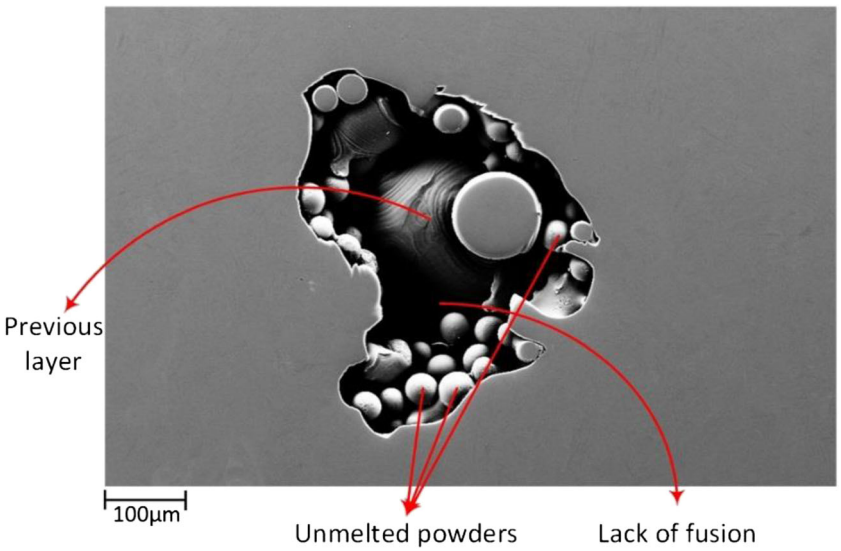

Fig. 5 Lack of fusion and big pore in the range of millimetre

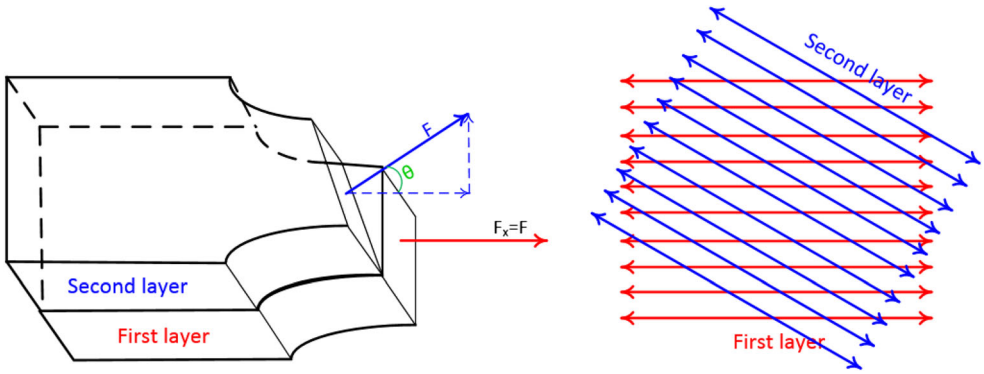

Fig. 6 Scan patterns and exerted forces

optimal build characteristics. It has been reported that within overlapping regions the value of roughness increases between 5 and 7 times compared to the centre of the track and that lower surface defects between subsequent layers result in higher tensile strength [41]

The increase in tensile strength can be explained by consideration of thermal properties. When increasing hatch space (Fig. 4**b** region A_B) radial acceleration and speed of melt flow increase and higher thermal conduction occur and a smoother surface is generated between subsequent layers due to a more homogeneous particle melting and wetting, which helps to improve the tensile strength [43]. Another reason for increasing tensile strength in higher hatch space is related to powder attachment in the overlap area. Larger overlap tends to increase previously fabricated track to absorb more energy and increase the temperature and generate wider heat affected zone and mush area therefore partially and unmelted particles attached to a solid interface and produce bigger pores [29].

Figures 3 and 4**c** show that laser power has more impact on strength compared to scanning pattern angle. By increasing scan pattern angle, the value of tensile strength increases. This effect is a well-known consequence of the build process and can be explained by the increases laser scan angle resulting in adjacent build lines being aligned away from the direction of the normal forces imposed during a typical tensile test. Increasing pattern angle leads to decreasing the tangential component of the forces and increases the tensile strength of the samples (Fig. 6). Additionally, it is believed that varying the scanning angle can allow for melt pool thermal control effects, which result in the increased tensile strength, particularly at higher laser powers. This would be due to the longer transition time of the laser allowing greater thermal relaxation of both the build layer and surface, at a threshold that results in reduced Marangoni's effects. Interestingly for laser powers of 93–97 W, the reverse trend is observed where tensile strength reduces for increased scan pattern angle and may be due to big

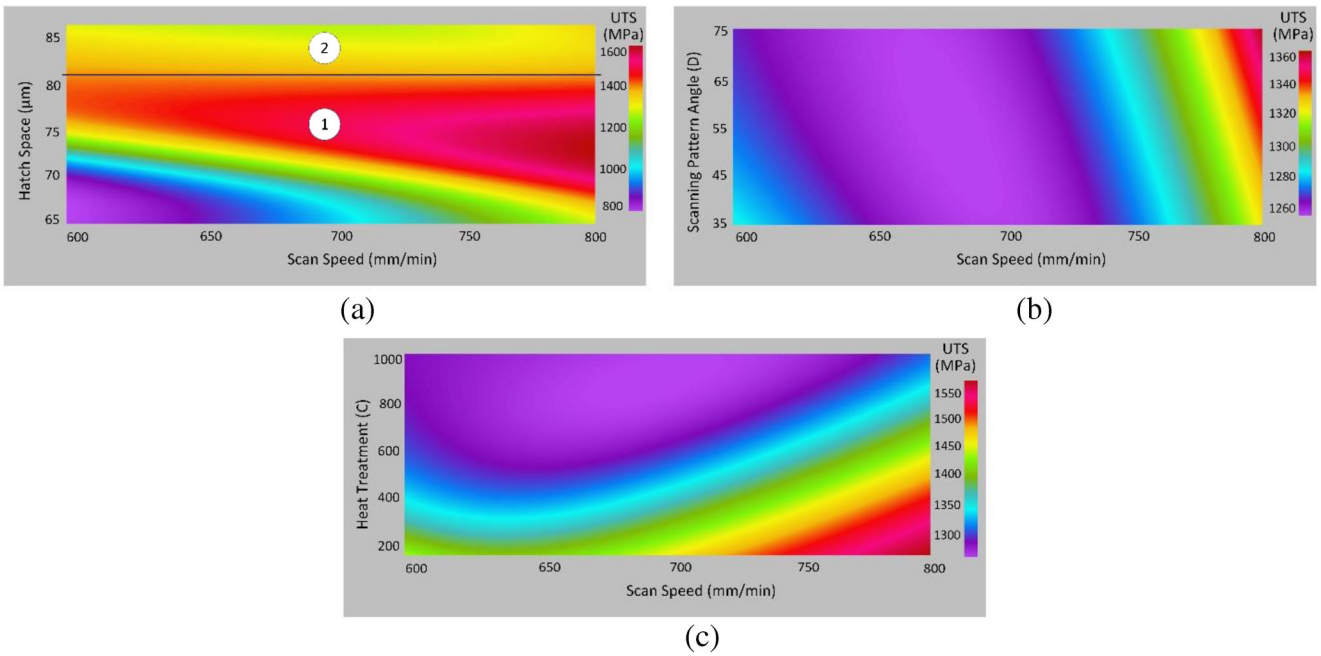

Fig. 7 Interaction of scan speed on other parameters

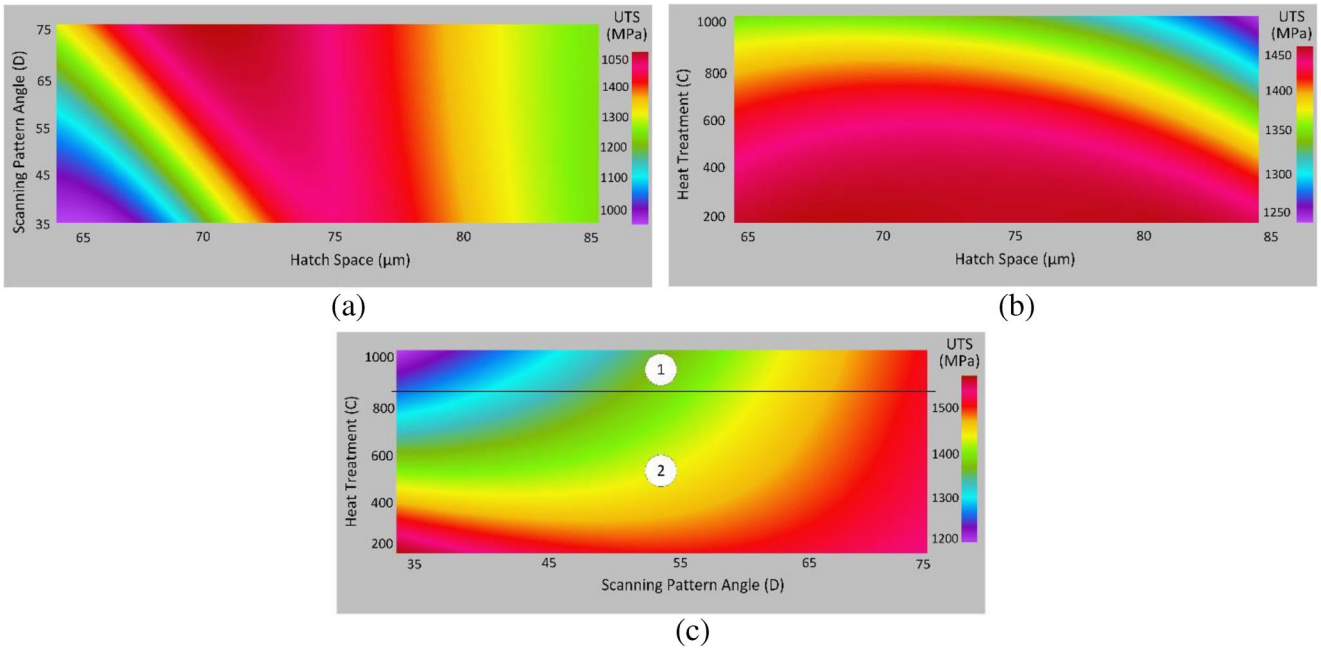

Fig. 8 Interaction of hatch space and scanning pattern on other parameters

pores (which are the results of lack of fusion) leading to non-linear and unpredictable behaviour.

Finally, Fig. 4**d** shows that in general, by increasing heat treatment temperature, the tensile properties decrease. However, in the optimum range of laser power (between 95 to 100 W), the tensile values did not present noticeable change (region 2). Similarly, in region 3, the value of tensile properties is constant by increasing heat treatment temperature. This behaviour demonstrates the greater influence of laser power on tensile strength compared to the effect of heat treatment. Interestingly, it is commonly believed that heat treatment is required for all materials to improve parts strain and clearly this is not be the case for Ti-6Al-4V for laser powers > 100 W in this study. In this alloy, the background phase is α with a small amount of β. α phase is stronger and β is more ductile. In higher than transition heat treatment (925 °C) due to low cooling rate, primary α retains itself and β is transformed to secondary α. Therefore, the microstructure is the mix of

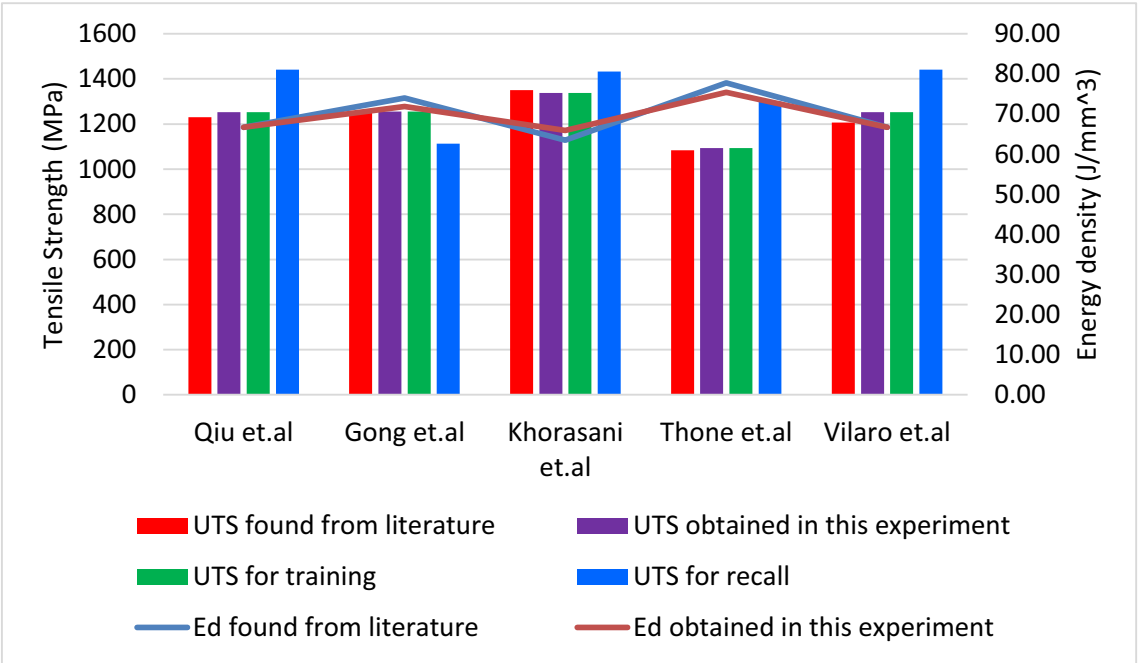

Fig. 9 Tensile strength of Ti-6Al-4V found from literature versus experimental, training and recall results for the same energy density [2, 14, 42, 51, 52]

lamellar, equiaxed and acicular. Formation of α-globular can also be related to partial remelting in the overlap of two hatches. Also, the formation of β is a direct function of low cooling rate and, in this case, β is transferred to secondary α lamellae and primary acicular α is changed to equiaxed α. This microstructure is extremely ductile compared to acicular structure and less strength [14].

4.4.2 Interaction of scan speed on hatch space, pattern angle and heat treatment

Figure 7**a**–**c** show contour plot graphs are illustrating the influence of scan speed against hatch spacing, scan pattern and heat treatment on tensile strength. Firstly, considering the combined influence of scan speed and hatch spacing, it was found the governing mechanisms dictating the overall tensile strength can be explained by considering the melt pool thermodynamics, as discussed previously. When considering the scan speed parameter, generally for lower speeds, the movement of fluid in the melt pool is equally slower. Dynamically two processes occur, firstly the fluid moves out from the centre carrying heat, which enhances heat transfer. Secondly, fluid in the outer regions experiences zero velocity, which in turn may result in keyhole defect formation. Simultaneously, due to the Marangoni effect, convection transfers the heat from the bottom of the keyholes to the surface and then outward, generating a larger width and 'cone-shape' melt pool that decreases the value of surface roughness. Based on Atthey [44] when Reynold's number is > 600, the melt pool becomes turbulent and a rough build surface is generated. This tends to increase the porosity and reduce the overall tensile strength. The Reynolds number can readily be calculated from Eq. 4

$$R_e = {}^{\rho u_m \omega}/_{\mu} \tag{4}$$

where ρ is density, u_m is scan speed, ω is melting pool width and μ is viscosity. By increasing scan speed, the cooling rate increases and viscosity decreases, which in turn decreases the melt pool width. Subsequently, the Reynolds number decreases, resulting in less turbulence within the melt pool, thereby reducing defects. This reduction in the defects results in increased tensile strength, which was observed in region 1 of Fig. 7**a**.

In the present experiment, the optimum value of hatch space ranged between 78 to 82 μm, with a relatively minor dependency on the scan speed. At hatch spacing > 82 μm (region 2, Fig. 7**a**), the tensile strength began to decrease, and is suspected to be related to lower part density (about 24.6%) resulting from the too large a hatch separation. Figure 7**b** shows a similar trend to Fig. 4**c** regarding the behaviour of laser pattern angle and resulting part tensile strength, where higher laser pattern angle results in an increased tensile strength.

Figure 7**c** reinforces the findings from Fig. 4**d**, which shows that tensile strength is a direct and indirect function of scan speed and heat treatment respectively. Ultimately, it was found that the highest strength was achieved for scan speeds of 730–760 mm/min. Beyond this, as the scan speed further increased, a linear increase in heat treatment temperatures was required to realise optimal tensile strength. This behaviour can be explained by consideration of the microstructural changes with respect to heat treatment. Firstly, during heat treatment, increases in the holding temperature lead to coarsening of the α-phase and a reduction in strength. In stress relieving (600 °C) and mill annealing (750 °C), a small fluctuation in the value of tensile strength was observed. When increasing heat treatment temperature in the range of 900–1050 °C, the percentage of β increases and equiaxed microstructures are formed and precipitation of beta on α' leads to decreasing tensile strength [15]. In α + β annealing due to low cooling rate, primary α retains itself and β is transformed to secondary α. Therefore, the microstructure is the mix of lamellar, equiaxed and acicular. Formation of α-globular may also be associated with partial remelting in the overlap region of two hatches. In this situation, β is transferred to secondary α lamellae and primary acicular α is changed to equiaxed α, resulting in lower part strength [28, 45–47]. In β annealing, this phase was transferred to secondary α and, by taking account of retaining primary α, the size of α phase increases and larger microstructures are obtained. In addition, due to a combination of higher temperatures and lower cooling rates, the self-diffusion coefficient increases and a homogeneous microstructure consisting of α is generated. Consequently, the value of α and grain size increases, while tensile strength decreases [14, 28, 48]. Decomposition of α'-martensite and nucleation of α precipitates at martensite plate boundaries result in enrichment of the surroundings with V as a β stabiliser, leading to the formation of equilibrium α + β phases mixtures. Combined these result in decreased tensile strength at higher heat treatment temperatures [15].

4.4.3 Interaction of other process parameters

Figure 8**a** shows that when using small hatch spacing and scanning pattern angle, the lowest tensile strength was obtained. This is believed to occur because, at lower hatch spacing, there is greater overlap between subsequent build tracks resulting in the production of microcrack defects, which reduce the part tensile strength. These microcracks occur due to the effect of incomplete homologous wetting and residual stresses produced by large solidification and undercooling of the melt pool. Equally, the tensile strength is reduced when using too large a hatch spacing due to a lower build density and reduced thermal penetration depth, which prevents remelting of the previous layers and results in weaker layer adhesion and build inhomogeneity [22]

Figure 8**b** shows that for hatch spacing between 65 and 75 μm optimal parts tensile strength is achieved from heat treatment value of approximately 650–700 °C. Beyond this hatch spacing (> 75 μm), the tensile strength is at a maximum for reduced heat treatment temperatures. These findings can be explained by referring to the microstructure morphology resulting from thermal management during the build process

Ti alloys have better tensile properties in equiaxed microstructure compared to lamellar, specifically with respect to ductility [17]. As the fabricated SLM Ti-6Al-4V has α' martensite, which has high strength, annealing due to heat treatment transfers it to $\alpha + \beta$, increasing the lamellae width, which reduces the tensile strength. It is reported that annealing at 700 and 800 °C only partially decomposes the α' phase in Ti-6Al-4V, meaning twins and dislocations remain, leading to lower ductility and a small reduction in strength [16]. Heat treatment effectively leads to transformation of the metastable martensite in the bi-phase $\alpha + \beta$ matrix, thereby enhancing tensile properties [49]. However, the final $\alpha + \beta$ morphology is highly dependent on the heat treatment temperature. When heat treatment has been carried out at temperatures higher than required for phase transformation, the beta phase is retained at grain at the boundary of alpha resulting in reduced tensile strength. When heat treatment is performed at 600–750 °C, this leads to the releasing of internal residual stresses and improves tensile properties [50].

Figure 8**c** shows better tensile strength was obtained with higher scanning pattern angles. Moreover, at higher scanning pattern angles, increased heat treatment temperatures were beneficial to maximising the tensile strength. Qiu et al. [42] showed hot isostatic pressing closes all pores, but still anisotropy remains in SLM parts. Layer-to-layer versus hatch-to-hatch effects are a dominant phenomenon on mechanical properties and anisotropy. This effect was observed in the current study and a higher pattern angle improved the tensile properties. This effect is more dominant in region 1, Fig. 8**c** which is related to decreasing tensile strength in heat treatment temperatures greater than approximately 850 °C. Therefore, reduction of the normal force which is exerted to the specimen with higher pattern angle will have more effect and tensile strength increases

4.5 Verification with the literature

In this section, data found in the literature is compared with the experimental findings, in addition to the test and cross-validation procedures. Figure 9 shows the tensile strength (UTS) and energy density from several comparative studies, examining a range of different build parameter conditions. It can be seen that this experiment produced similar values with the literature with respect to energy density. It means that the value of UTS for training and recall should be close to the obtained UTS in this experiment and also close to the values that were found from the literature. However, the experimental values in this research have some differences with the literature which is most likely related to the nature of each machine. This figure shows good accuracy was obtained for both training and recall procedures, which proves the generality of the proposed ANN model.

5 Conclusion

This investigation showed how changing the SLM process parameters affect the value of tensile strength when printing Ti-6Al-4V. The experiment was guided by an ANN model, which was cross-validated by generated data sets and further approved by similar tests from the literature. The study showed that ANNs have the capability to model nonlinear problems such as process parameters in additive manufacturing. Analysis showed that laser power is the most influential build parameter

Table 5 Experimental values of tensile and elongations

Test number	Breaking elongation (%)	Average tensile strength	Test number	Breaking elongation (%)	Average tensile strength
1	2.37	932.15	14	4.10	948.26
2	3.67	1338.27	15	3.20	1121.28
3	9.00	1413.65	16	3.83	893.65
4	7.28	1028.73	17	3.37	1173.70
5	3.76	755.55	18	3.36	1394.14
6	4.72	1093.50	19	9.96	1253.18
7	5.73	1059.00	20	5.18	1064.54
8	3.46	1203.75	21	10.50	1255.90
9	3.17	1255.15	22	6.42	1106.97
10	9.64	1425.28	23	6.19	905.94
11	3.67	1428.07	24	3.57	1330.39
12	8.41	1251.04	25	3.93	1506.74
13	4.57	1079.11			

on the value of tensile strength, followed by scan speed, heat treatment, hatch spacing and the laser pattern angle. The results of interaction diagrams showed that laser power and hatch spacing should be kept at optimal values to generate better tensile strength (756.87 to 1537.67 MPa). Equally, it was discovered that the higher the scan speed, the lower the tensile strength. Heat treatment also has a profound effect on tensile properties, where higher heat treatment temperatures result in lower tensile properties. Combining process parameters ultimately revealed nonlinear behaviour on tensile properties. However, this research showed an effective means by which process parameters coupling with heat treatment can improve tensile strength in a cost-effective and practical way in a widely utilised commercial AM system.

Appendix

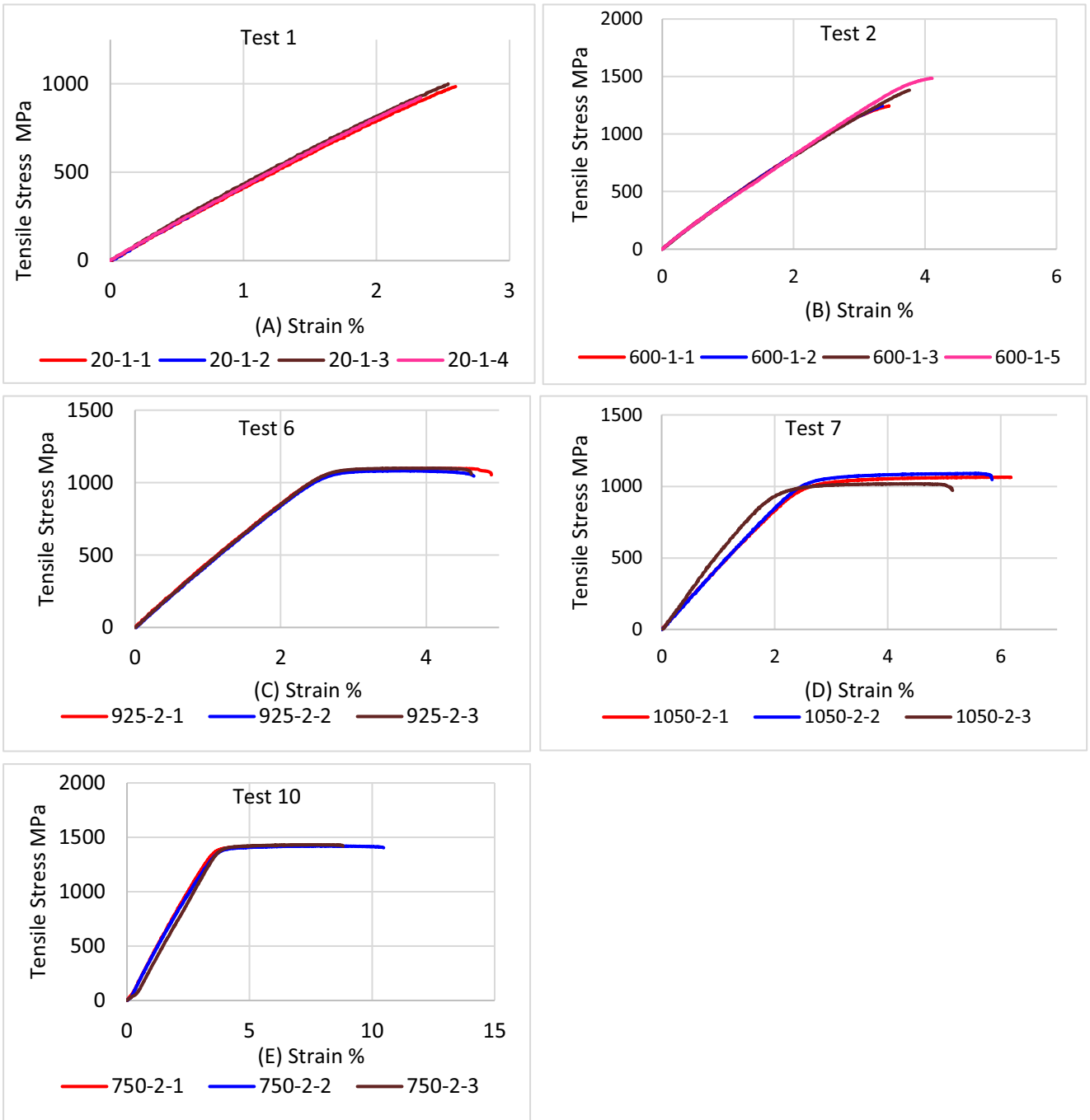

Fig. 10 Stress strain curves for test samples 1, 2, 6, 7 and 10

References

1. Khorasani A, Gibson I, Goldberg M, Littlefair G (2017) Production of Ti-6Al-4V acetabular shell using selective laser melting: possible limitations in fabrication. Rapid Prototyp J 23(1):110–121
2. Gong H, Rafi K, Gu H, Janaki Ram GD, Starr T, Stucker B (2015) Influence of defects on mechanical properties of Ti–6Al–4V components produced by selective laser melting and electron beam melting. Mater Des 86:545–554
3. Kadirgama K, Harun WSW, Tarlochan F, Samykano M, Ramasamy D, Azir MZ, Mehboob H (2018) Statistical and optimize of lattice structures with selective laser melting (SLM) of Ti6AL4V material. Int J Adv Manuf Technol 97(1):495–510
4. Zhang P, Zhang DZ, Peng D, Li Z, Mao Z (2018) Rolling contact fatigue performance evaluation of Ti–6Al–4V parts processed by selective laser melting. Int J Adv Manuf Technol 96(9):3533–3543
5. Boschetto A, Bottini L, Veniali F (2018) Surface roughness and radiusing of Ti6Al4V selective laser melting-manufactured parts conditioned by barrel finishing. Int J Adv Manuf Technol 94(5): 2773–2790
6. Khorasani AM (2017) The selected laser melting production and subsequent post-processing of Ti-6Al-4V prosthetic acetabular. Deakin University
7. Gibson I, Rosen DW, Stucker B (2015) Additive manufacturing technologies. Springer
8. Teng C, Pal D, Gong H, Zeng K, Briggs K, Patil N, Stucker B (2017) A review of defect modeling in laser material processing. Addit Manuf 14:137–147
9. Gong H et al (2014) Analysis of defect generation in Ti–6Al–4V parts made using powder bed fusion additive manufacturing processes. Addit Manuf 1:87–98
10. Gong H, et al. (2014) Melt pool characterization for selective laser melting of Ti-6Al-4V pre-alloyed powder. In Solid freeform fabrication symposium
11. Prashanth KG, Scudino S, Eckert J (2017) Defining the tensile properties of Al-12Si parts produced by selective laser melting. Acta Mater 126:25–35
12. Hassn AH, Christopher S, Liang H (2018) Effect of build orientation on the surface quality, microstructure and mechanical properties of selective laser melting 316L stainless steel. Rapid Prototyp J 24(1):9–17
13. Rao H, Giet S, Yang K, Wu X, Davies CHJ (2016) The influence of processing parameters on aluminium alloy A357 manufactured by selective laser melting. Mater Des 109:334–346
14. Khorasani A, Gibson I, Goldberg M, Littlefair G (2017) On the role of different annealing heat treatments on mechanical properties and microstructure of selective laser melted and conventional wrought Ti-6Al-4V. Rapid Prototyp J 23(2):295–304
15. Yadroitsev I, Krakhmalev P, Yadroitsava I (2014) Selective laser melting of Ti6Al4V alloy for biomedical applications: temperature monitoring and microstructural evolution. J Alloys Compd 583: 404–409
16. Cao S, Chu R, Zhou X, Yang K, Jia Q, Lim CVS, Huang A, Wu X (2018) Role of martensite decomposition in tensile properties of selective laser melted Ti-6Al-4V. J Alloys Compd 744:357–363
17. Cai C, Gao X, Teng Q, Li M, Pan K, Song B, Yan C, Wei Q, Shi Y (2018) A novel hybrid selective laser melting/hot isostatic pressing of near-net shaped Ti-6Al-4V alloy using an in-situ tooling: interfacial microstructure evolution and enhanced mechanical properties. Mater Sci Eng A 717:95–104
18. Savalani MM, Pizarro JM (2016) Effect of preheat and layer thickness on selective laser melting (SLM) of magnesium. Rapid Prototyp J 22(1):115–122
19. Yadroitsev I, Krakhmalev P, Yadroitsava I, Johansson S, Smurov I (2013) Energy input effect on morphology and microstructure of selective laser melting single track from metallic powder. J Mater Process Technol 213(4):606–13
20. Gustmann T, Neves A, Kühn U, Gargarella P, Kiminami CS, Bolfarini C, Eckert J, Pauly S (2016) Influence of processing parameters on the fabrication of a Cu-Al-Ni-Mn shape-memory alloy by selective laser melting. Addit Manuf 11:23–31
21. Dai D, Gu D, Zhang H, Xiong J, Ma C, Hong C, Poprawe R (2018) Influence of scan strategy and molten pool configuration on microstructures and tensile properties of selective laser melting additive manufactured aluminum based parts. Opt Laser Technol 99:91–100
22. Spierings A, Herres N, Levy G (2011) Influence of the particle size distribution on surface quality and mechanical properties in AM steel parts. Rapid Prototyp J 17(3):195–202
23. Joguet D, Costil S, Liao H, Danlos Y (2016) Porosity content control of CoCrMo and titanium parts by Taguchi method applied to selective laser melting process parameter. Rapid Prototyp J 22(1): 20–30
24. Bikas H, Stavropoulos P, Chryssolouris G (2016) Additive manufacturing methods and modelling approaches: a critical review. Int J Adv Manuf Technol 83(1–4):389–405
25. ASTM (2014) Additive Manufacturing Titanium-6 Aluminum-4 Vanadium with Powder Bed Fusion. ASTM. p. 1–9
26. Roy RK (2010) A primer on the Taguchi method. Society of Manufacturing Engineers
27. Khorasani AM, Gibson I, Goldberg M, Littlefair G (2016) A survey on mechanisms and critical parameters on solidification of selective laser melting during fabrication of Ti-6Al-4V prosthetic acetabular cup. Mater Des 103:348–355
28. Boyer R, Welsch G, Collings EW (1994) Materials properties handbook: titanium alloys. ASM international
29. Khorasani AM, Jalali Aghchai A, Khorram A (2011) Chatter prediction in turning process of conical workpieces by using case-based resoning (CBR) method and taguchi design of experiment. Int J Adv Manuf Technol 55(5–8):457–464
30. Ruck DW et al (1990) The multilayer perceptron as an approximation to a Bayes optimal discriminant function. IEEE Trans Neural Netw **1**(4):296–298
31. Khorasani AM, Yazdi MRS, Safizadeh MSJIJOE (2011) Tool Life Prediction in Face Milling Machiningof 7075 Al by Using Artificial Neural Networks (ANN) and Taguchi Design of Experiment (DOE). Int J Eng Technol **3**(1):30
32. Khorasani A, Yazdi MRS (2015) Development of a dynamic surface roughness monitoring system based on artificial neural networks (ANN) in milling operation. Int J Adv Manuf Technol:1–11
33. Mertens A, Reginster S, Paydas H, Contrepois Q, Dormal T, Lemaire O, Lecomte-Beckers J (2014) Mechanical properties of alloy Ti–6Al–4V and of stainless steel 316L processed by selective laser melting: influence of out-of-equilibrium microstructures. Powder Metall 57(3):184–189
34. Khorasani A, Yazdi MRS (2017) Development of a dynamic surface roughness monitoring system based on artificial neural networks (ANN) in milling operation. Int J Adv Manuf Technol 93(1–4):141–151
35. Pupo Y, Monroy KP, Ciurana J (2015) Influence of process parameters on surface quality of CoCrMo produced by selective laser melting. Int J Adv Manuf Technol 80(5–8):985–995
36. Rafi H et al (2013) Microstructures and mechanical properties of Ti6Al4V parts fabricated by selective laser melting and electron beam melting. J Mater Eng Perform 22(12):3872–3883

37. Safdar A, He HZ, Wei LY, Snis A, Chavez de Paz LE (2012) Effect of process parameters settings and thickness on surface roughness of EBM produced Ti-6Al-4V. Rapid Prototyp J 18(5):401–408
38. Berthier J (2012) Micro-drops and digital microfluidics. 2nd ed. William Andrew
39. Malkin AY, Isayev AI (2017) Rheology: concepts, methods, and applications. 3rd ed. Elsevier
40. Khorasani AM, Gibson I, Ghaderi AR (2018) Rheological characterization of process parameters influence on surface quality of Ti-6Al-4V parts manufactured by selective laser melting. Int J Adv Manuf Technol 97(9):3761–3775
41. Averyanova M, Cicala E, Bertrand P, Grevey D (2012) Experimental design approach to optimize selective laser melting of martensitic 17-4 PH powder: part I–single laser tracks and first layer. Rapid Prototyp J 18(1):28–37
42. Qiu C, Adkins NJE, Attallah MM (2013) Microstructure and tensile properties of selectively laser-melted and of HIPed laser-melted Ti–6Al–4V. Mater Sci Eng A 578:230–239
43. Ahn IH, Moon SK, Hwang J, Bi G (2017) Characteristic length of the solidified melt pool in selective laser melting process. Rapid Prototyp J 23(2):370–81
44. Atthey D (1980) A mathematical model for fluid flow in a weld pool at high currents. J Fluid Mech 98(4):787–801
45. Li X et al (2015) Effect of substrate temperature on the interface bond between support and substrate during selective laser melting of Al–Ni–Y–Co–La metallic glass. Mater Des **65**:1–6
46. Sieniawski J, Ziaja W, Kubiak K, Motyka M (2013) Microstructure and mechanical properties of high strength two-phase titanium alloys. Titanium Alloys-Advances in Properties Control. InTech Open. https://doi.org/10.5772/56197
47. Jovanović M et al (2006) The effect of annealing temperatures and cooling rates on microstructure and mechanical properties of investment cast Ti–6Al–4V alloy. Mater Des 27(3):192–199
48. ASM Hanbook Volume 2 (2010) Properties and Selection: Nonferrous and specialpurpose Materials, Titanium and Titanium Alloy Castings Product Application Vol. 2. ASTM international, America
49. Facchini L, Magalini E, Robotti P, Molinari A, Höges S, Wissenbach K (2010) Ductility of a Ti-6Al-4V alloy produced by selective laser melting of prealloyed powders. Rapid Prototyp J 16(6):450–459
50. Simonelli M, Tse YY, Tuck C (2014) Effect of the build orientation on the mechanical properties and fracture modes of SLM Ti–6Al–4V. Mater Sci Eng A 616:1–11
51. Vilaro T, Colin C, Bartout J-D (2011) As-fabricated and heat-treated microstructures of the Ti-6Al-4V alloy processed by selective laser melting. Metall Mater Trans A 42(10):3190–3199
52. Thöne M, Leuders S, Riemer A, Tröster T, Richard H (eds) (2012). Influence of heat-treatment on Selective Laser Melting products–eg Ti6Al4V. Solid freeform fabrication symposium SFF, Austin Texas